2018

Sedimentary Catalysis of Radiolytic Hydrogen Production

Justine Flore Sauvage
University of Rhode Island, justine_sauvage@uri.edu

SEDIMENTARY CATALYSIS OF RADIOLYTIC HYDROGEN PRODUCTION

BY

JUSTINE FLORE SAUVAGE

A DISSERTATION SUBMITTED IN PARTIAL FULFILLMENT OF THE REQUIREMENTS FOR THE DEGREE OF

DOCTOR OF PHILOSOPHY

IN

OCEANOGRAPHY

UNIVERSITY OF RHODE ISLAND

2018

DOCTOR OF PHILOSOPHY DISSERTATION

OF

JUSTINE FLORE SAUVAGE

APPROVED:

Dissertation Committee:

Major Professor Steven D'Hondt

Arthur Spivack

David Fastovsky

Nasser H. Zawia

DEAN OF THE GRADUATE SCHOOL

UNIVERSITY OF RHODE ISLAND

2018

ABSTRACT

Hydrogen (H_2) and oxidants (O_2 and H_2O_2) are naturally produced by radiolysis of water in any environment where water is bombarded by α, β, and γ radiation generated during radioactive decay. The production of radiolytic H_2 in aqueous solutions and in some monomineral-water mixtures has been extensively studied. However, yields of radiolytic products in natural materials remain largely unexplored.

Quantification of radiolytic production in common geological materials is critical to assess the importance of water radiolysis as source of microbial reductants and oxidants in water-containing subsurface environments. Knowledge of radiolytic production is also fundamental for the nuclear industry, as maintenance and development of nuclear reactors, long-term disposal of radioactive waste and management of mixed-waste storage tanks are intricately associated with radiolysis products.

We experimentally quantified H_2 yields for α- and γ-irradiation of pure water, seawater, and slurries of marine sediment, montmorillonite, and two natural zeolites (mordenite and clinoptilolite) widely used in the nuclear industry. The sediment samples include the dominant types found in the global ocean (abyssal clay, nannofossil-bearing clay [marl], clay-bearing diatom ooze, and nannofossil ooze). These experiments demonstrate that all common types of marine sediment and both zeolites catalyze radiolytic H_2 production. Hydrogen yields [$G(H_2)$] from water radiolysis differ from one geological material to another. They range between 3.43 and 37.54 molecules H_2 $100eV^{-1}$ for α-particles and and 0.27 and 1.96 molecules H_2 $100eV^{-1}$ for γ-rays. Abyssal clay, earth's most widespread marine sediment type, exhibits the highest yield amplification when exposed to α-particles with an average factor increase of 18 relative to pure water. Siliceous ooze and abyssal clay exhibit the highest H_2 yields when exposed to γ-rays,

increasing production by factors of up to 8 and 4, respectively. Calcareous ooze (factor 5 amplification) and lithogeneous sediment (17% amplification) exhibit the smallest yield amplification under α-particle and γ-rays irradiation, respectively. Zeolite mineral slurries increase $G(H_2)$ for α- and γ-irradiation by factors of 13 and 4, respectively (similar to abyssal clay). Our results show that substrate chemistry and specific surface area are the main factors that control radiolytic H_2 production.

The mineral-catalysis of radiolytic H_2 production has significant implications for: (i) sustenance of Earth's subsurface microbial ecosystems (ii) habitability of other planetary bodies, and (iii) nuclear industrial activities.

In electron equivalents per unit area, radiolytic H_2 production in marine sediment locally produces as much electron donor (food) as photosynthetic carbon fixation in the ocean. Although small relative to global photosynthetic biomass production, sediment-catalyzed production of radiolytic products is significant in the subseafloor. Our analysis of 9 sites in the North Atlantic, North and South Pacific suggests that H_2 is the primary microbial fuel in oxic organic-poor sediment older than a few million years. At these sites, calculated radiolytic H_2 consumption rates are more than an order of magnitude higher than *in situ* organic-matter oxidation rates. Radiolytic H_2 is also a significant microbial electron donor in anoxic marine sediment older than a few million years. Oxidants from water radiolysis (O_2 and H_2O_2) are significant electron acceptors in both oxic and anoxic sediment throughout the ocean.

Discovery and quantification of the catalytic effect of clays and zeolites on radiolytic H_2 production reveals the potential risk of using geological materials for remediation and long-term disposal of nuclear waste without consideration of their catalytic potential.

ACKNOWLEDGMENTS

I want to, first of all, thank the University of Rhode Island and the GSO community for providing a wonderful work environment. I also want to acknowledge the National Science Foundation, the National Aeronautics and Space Administration, The Center for Deep Dark Energy Biosphere Investigations and the International Ocean Discovery Program because without their financial support this work would not have happened.

To Annie Foppert, Annie Hartwell, Coline Dony, Ashton Flinders, David DeVleeschouwer, and François Paquay for being fantastic colleagues, but also great friends. Your kindness and support knows no bounds.

To Perry (and Wombat), who didn't mind when I lost my mind and never underestimated the healing powers of mythological characters, good food, and E. Matunuck sunsets. Your company and kindness kept me going and I thank you for it.

To Professeur Fastovsky, thank you for your enthusiasm on this project and keeping my orthographe in check. And to Rebecca Robinson and Anne Veeger, thank you for being on my committee.

To Art, thank you for always double-checking my calculations, units and use of the active voice. You taught me a lot both on land and at sea.

To Phillipe Claeys thank you for having the vision.

And finally, to Steve, it's been an honor and a great journey to work with you. Thank you for this opportunity and for always supporting me in my dynamic and sometimes unpredictable professional aspirations. I will make sure Belgian chocolates keep coming your way!

DEDICATION

To *la Famille Sauvage*

PREFACE

This dissertation is a combination of three individual manuscripts (dissertation chapters) in preparation for publication in scientific journals. The first manuscript, "The Contribution of Water Radiolysis to Subseafloor Sedimentary Life", is prepared for submission to *Science* in Spring 2018. The second and third manuscript, "Production of Radiolytic H_2 in Aqueous Slurries of Marine Sediment, Zeolite and Montmorillonite under γ-ray Irradiation" and "H_2 production by α-particle water radiolysis in marine sediment, clinoptilolite, mordenite and montmorillonite slurries" will respectively be submitted to the *Journal of Physical chemistry C* (C2: Surfaces, Interfaces, Porous Materials, and Catalysis) and *Environmental Science & Technology*, following publication of the first manuscript.

TABLE OF CONTENT

LIST OF FIGURES

LIST OF TABLES

TABLE PAGE

MANUSCRIPT 1

The contribution of water radiolysis to marine sedimentary life

Justine F. Sauvage[1], Ashton Flinders[2], Arthur J. Spivack[1], Robert Pockalny[1], Ann G. Dunlea[3*], Chloe H. Anderson[3], David C. Smith[1], Richard W. Murray[3], and Steven D'Hondt[1]

In preparation for *Science*

---

[1] *Graduate School of Oceanography, University of Rhode Island, Narragansett, RI 02882, USA.*

[2] *United States Geological Survey, Menlo Park, Ca.*

[3] *Department of Earth and Environment, Boston University, Boston, MA 02215, USA*

[*] *now at Woods Hole Oceanographic Institution, Woods Hole, MA 02543, USA.*

1. Abstract

Water radiolysis is a continuous source of hydrogen (H_2) and hydrogenperoxide (H_2O_2) in wet sediment and rock. We show that all marine sediment efficiently catalyzes H_2 production by water radiolysis, amplifying H_2 yields by up to a factor of 27 relative to pure water, depending on sediment composition. In electron equivalents per unit area, radiolytic H_2 production in marine sediment locally produces as much electron donor (food) as photosynthetic carbon fixation in the overlying ocean. Comparison to *in situ* organic oxidation rates suggests that water radiolysis is the principal source of electron donors (H_2) and electron acceptors for microbial communities in all marine sediment older than a few million years.

One sentence summary: Marine sediment catalyzes radiolytic H_2 and H_2O_2 production, rendering radiolysis a significant energy source for subseafloor sedimentary ecosystems.

1.2. Main text

H_2 and H_2O_2 are continuously generated in wet sediment and rock from splitting of water [$2H_2O \rightarrow H_2 + H_2O_2$] by radiation from decay of naturally occurring radionuclides [^{238}U, ^{235}U, ^{232}Th, and ^{40}K] *(1, 2, 3)*. The H_2O_2 typically rapidly degrades to O_2 and H_2O *(4, 5)*. These radiolytic products constitute a continuous source of energy for microbial ecosystems in subsurface environments *(6)*. Previous studies have identified radiolytic H_2 as the primary electron donor (food) for microbial ecosystems of continental aquifers kilometers below Earth's surface *(4, 7)*. Radiolytic products (oxidants and H_2) have also been suggested to be significant for sustenance of microbial communities in sediment meters beneath the seafloor *(8, 9)* and subsurface environments of other planets *(3, 10, 11)*. Despite these suggestions, the extent to which marine sedimentary ecosystems rely on radiolytic products has been unclear, because (i) radiolytic chemical yields in natural environments have been poorly constrained, and (ii) organic matter and oxidants from the surface photosynthetic world are ubiquitous in marine sediment. Even where photosynthetically produced organic matter and oxidants are absent, such as in deep continental aquifers and the subsurface of other planets, understanding is hampered by uncertain knowledge of radiolytic chemical yields in natural environments.

Radiolytic yields in pure water are well constrained *(12, 13)*. Previous γ-radiation studies indicate that some solid materials in aqueous environments amplify radiolytic production *(14)*. For example, some minerals, including quartz, zirconium dioxide, cerium dioxide, uranium dioxide, pyrite, and mordenite, when dispersed in water and exposed to γ-rays increase radiolytic H_2 production by up to a factor of 10 relative to pure water *(10, 14, 15, 16)*. However, the effect of mineralogically complex natural materials on H_2 yields is previously unexplored. Here we experimentally quantify the production of radiolytic H_2

in some of Earth's most widespread geological materials – the seawater-saturated marine sediment types that collectively cover ~70% of Earth's surface. These experiments demonstrate that all common types of marine sediment catalyze radiolytic H_2 production, amplifying yields by as much as a factor of 27, depending on sediment lithology. Building on this experimental data, we calculate the first global budgets of radiolytic H_2 and oxidant production in marine sediment, and quantify their contributions to subseafloor microbial metabolism.

We experimentally quantified H_2 yields for α- and γ-irradiation of pure water, seawater and seawater-saturated marine sediment at typical abyssal clay porosity (83%). The samples include all sediment types abundant in the global ocean (abyssal clay, nannofossil-bearing clay [marl], clay-bearing siliceous ooze, calcareous ooze and lithogenous). Details of samples and methods are in the *Supplementary Information*.

H_2 production increases linearly with absorbed α- and γ-ray-dose, for pure water, seawater, and marine sediment slurries (*Supplementary Information*). Energy-normalized radiolytic H_2 yields, denoted by $G(H_2)$ [molecules H_2 100 eV^{-1}] *(1)*, in seawater are indistinguishable from those in pure water, within a 90% confidence limit, for α-irradiation and for γ-irradiation. In contrast, $G(H_2)$ values of marine sediment slurries are consistently higher than those for pure water, with the magnitude depending on lithology and radiation type.

The catalytic effect of marine sediment on radiolytic yield is significant for both α- and γ-irradiation, but much larger for α-irradiation (**Figure 1.1**). Alpha-irradiation $G(H_2)$ values for slurries of abyssal clay were more than an order of magnitude higher than for pure water (ranging between factors of 13 and 27 increase). On average, clay-bearing

siliceous ooze and calcareous marl increased $G(H_2)$ for α-irradiation by factors of 15 and 12, respectively. Nannofossil ooze increased yields by a factor of 5 for α-irradiation. Clay-bearing siliceous ooze, and abyssal clay amplified $G(H_2)$ by factors of 8 and 4, respectively for γ-irradiation. Nannofossil ooze and marl slurries doubled $G(H_2)$ for γ-irradiation.

H_2 from radiolysis of pure H_2O is stoichiometrically balanced by H_2O_2 production *(17)*. These relatively stable products culminate from reactions in which radicals (H•, OH•, e_{aq}^-, and HO_2•) are intermediates following H_2O dissociation *(1)*. Zeolite minerals and some oxides (e.g. Al_2O_3) effectively adsorb H_2O_2 and OH radicals *(14, 18, 19)*. Dissolved H_2O_2 is unstable and its decomposition ($2H_2O_2 \rightarrow 2H_2O + O_2$) is catalyzed by many different materials *(4,5)*. For example, metal oxides (e.g., goethite and Fe-Mn oxyhydroxides) clays, silica and zeolites common in marine sediment are highly active catalysts of H_2O_2 decomposition to H_2O and O_2 *(4, 20, 21)*. Catalytic or radiation-induced decomposition of the adsorbed H_2O_2 and OH radicals has three important consequences for water radiolysis: (i) removal of OH radicals, the dominant scavenger of H_2 during the rapid sequence of reactions that typically follows water radiolysis (i.e. $H_2 + 2{\bullet}OH \rightarrow 2H_2O$), (ii) production of H radicals and thus additional H_2 ($\bullet H + \bullet H \rightarrow H_2$), and (iii) production of O_2 *(18, 19)*. In sum, common minerals in deep-sea sediment have the integrated effect of increasing H_2 and O_2 radiolytic yields and decreasing net H_2O_2 yields.

Depending on sediment type, we calculate that 40-60% of the energy absorbed by water in wet marine sediment forms radiolytic H_2 and H_2O_2 (*Supplementary Information*). This indicates that marine sediment is remarkably efficient at catalyzing production of H_2 and H_2O_2 from water radiolysis.

These results demonstrate that (i) all common marine sediment types efficiently catalyze radiolytic H_2 production, and (ii) the magnitude of this catalysis depends on

sediment composition and radiation type. While the mechanisms by which mineral grains catalyze radiolytic H_2 production are not fully resolved, potential controlling factors include chemical composition, crystal structure, specific surface area and the efficiency of energy transfer from the solid to the water *(14)*.

Many microorganisms can directly or indirectly utilize radiolytic H_2 and/or radiolytic H_2O_2 for energy-yielding reactions *(6, 22)*. H_2O_2 is unstable and quickly decomposes to O_2 in due to spontaneous reactions or mineral catalysts (*4, 5*). Microorganisms can metabolize the degradation products of H_2O_2. For example, some lithoautrophic communities are fueled by oxidation of H_2 with O_2 [i.e. $H_2 + ½O_2 \rightarrow H_2O$, referred to as the *Knallgas* reaction] *(6)*. Some bacteria, including *Escheria coli*, can directly metabolize H_2O_2 using cyctochrome c peroxidase as a respiratory enzyme *(22)*.

To assess the contribution of water radiolysis to global bioenergy fluxes, we quantify the global production of radiolytic H_2 and H_2O_2 in marine sediment (**Figure 1.2A**). This calculation spatially integrates sedimentary radiolytic H_2 production rates *(2)* derived from (i) our experimentally constrained radiolytic H_2 yields for the principal marine sediment types, (iii) measured radioactive element content of sediment cores in three ocean basins (North Atlantic, North and South Pacific), and global distributions of (iv) seafloor lithology, (v) sediment porosity, and (vi) sediment thickness [*see supplementary information*] *(23, 24, 25)*.

At 83% porosity, radiolytic H_2 production rates, normalized to sediment volume, differ by one order of magnitude from one lithology to another, with highest rates in abyssal clay ($3.41 – 5.23*10^{-11}$ mol H_2 cm^{-3} yr^{-1}, equivalent to $6.82*10^{-11}$-$1.05 *10^{-10}$ mol electrons cm^{-3} yr^{-1}) and lowest rates in nannofossil ooze ($1.20 – 8.32*10^{-12}$ mol H_2 cm^{-3} yr^{-1}, equivalent to $2.40* 10^{-12} – 1.66*10^{-11}$ mol electrons cm^{-3} yr^{-1}). This large range is

predominantly due to different $G(H_2)$ values and different U, Th and K concentrations in the different lithologies. The calculated global radiolytic H_2 production rate in marine sediment is $2.1*10^{14}$ mol H_2 yr^{-1} (equivalent to $4.2*10^{14}$ mol electrons yr^{-1}). This global rate is ~1/1000 the global rate of photosynthetic organic-carbon production in the surface ocean [$3.1*10^{16}$ mol C yr^{-1}, equivalent to $1.2*10^{17}$ mol electrons yr^{-1}] (*26*). However, in electron equivalents per unit area, radiolytic H_2 production in marine sediment locally produces as much electron donor as photosynthetic carbon fixation in the ocean (**Figure 1.2B**, *Supplementary Information*).

To assess the importance of mineral-catalyzed radiolytic products for sustaining subseafloor sedimentary ecosystems, we quantitatively examine the importance of radiolytically produced H_2 and H_2O_2 for microbial catabolism at 9 sites where deep subseafloor sediment is oxic and 7 sites where deep subseafloor sediment is anoxic. We first assess the importance of radiolytic H_2 as an electron donor in oxic sediment, where organic matter concentrations are low but electron acceptors are abundant (*28*), and in anoxic sediment, where organic matter is relatively abundant but electron acceptors other than dissolved inorganic carbon (DIC), and at some sites sulfate (SO_4^{2-}), are rare. We then assess the importance of oxidizing power from radiolytic H_2O_2 as an electron acceptor in oxic and anoxic sediment.

Despite continual production by radiolysis, dissolved H_2 concentrations are mostly below detection [1-5 nM H_2] at the oxic sites (*21*, *28*) and low (1-80 nM H_2) at the anoxic sites (**Figure 1.3**, *Supplementary Information*). *In situ* H_2 concentrations are generally 2 to 5 orders of magnitude lower than concentrations expected from radiolytic production in the absence of H_2-consuming reactions (**Figure 1.3**, *Supplementary Information*). These low concentrations indicate that H_2 consumption is essentially equal to radiolytic H_2

production throughout these sedimentary sequences. The simplest explanation is microbial H_2 oxidation at all depths, since the *in situ* Gibbs energy of H_2 oxidation is energy-yielding at the H_2 detection limit throughout these sequences (*Supplementary Information*).

To quantify the potential importance of radiolytic H_2 as an electron donor for oxic subseafloor ecosystems, we compare vertical distributions of radiolytic H_2 consumption (assumed equal to production) to vertical distributions of net O_2 consumption at each site. Comparison of net O_2 reduction to net nitrate (NO_3^-) production suggests that net O_2 reduction primarily results from oxidation of buried marine organic matter with a typical oceanic C:N ratio (*27*). This inference is consistent with consumption of radiolytic H_2O_2 and its decomposition product O_2 in parallel with radiolytic H_2, resulting in the contribution of radiolytic H_2 oxidation to gross respiration, but not net O_2 consumption. Given these relations, the ratio of radiolytic H_2 production to net O_2 reduction [expressed in electron equivalents transferred per mol H_2 oxidized and mol O_2 reduced, respectively (mol e^- cm_{sed}^{-3} yr^{-1})] is a measure of the extent to which radiolytic H_2 serves as the primary electron donor for this aerobic subseafloor ecosystem (**Figure 1.4A**). To the extent that radiolytic H_2 also contributes to net O_2 consumption (e.g., if some radiolytic H_2O_2 is consumed by mineral oxidation), this ratio overestimates organic oxidation rate and underestimates the role of radiolytic H_2 as an electron donor.

In oxic sediment deposited during the last few million years, this ratio is generally below 1.0 (~0.01 to 0.8), indicating that microbial respiration in relatively young oxic sediment is primarily based on oxidation of organic matter (**Figure 1.4A**). In older oxic sediment, this ratio is generally above 1.0 (~1 to 86), implying that radiolytic H_2 is the primary electron donor. The rate of radiolytic H_2 production is more than an order of

magnitude higher than the rate of organic-fueled O_2 reduction in the oldest oxic sediment (starting at 11 Ma at Site 12 in the North Atlantic, 10 Ma at Site EQP-11 in the North Pacific and 41 Ma at Site U1370 in the South Pacific Gyre, [*21, 27*]). The consistency of this result in the North Atlantic, North Pacific and South Pacific suggests that radiolytic H_2 is the principal microbial fuel in oxic marine sediment older than a few Ma.

To evaluate radiolytic H_2 as a microbial fuel in anoxic sediment, we compare radiolytic production rates to DIC production rates for 7 sites from the Equatorial Pacific, South Pacific, Peru Margin and Bering Sea (**Figure 1.4B**). For this comparison, we assume DIC to be the primary oxidized product of organic-fueled catabolism. In the anoxic sediment younger than a few Ma, this ratio is generally below 1, indicating that organic matter is the primary electron donor. However, as at the oxic sites, in anoxic sediment older than a few Ma, electron equivalents of radiolytic H_2 production generally exceeds electron equivalents of net DIC production by factors of 1.2 (starting at 2.5 Ma at Eastern Equatorial Pacific Site 1226) to 22 (starting at 15 Ma at South Pacific Site U1371) [**Figure 1.4B**]. The consistency of this result in the South Pacific, Equatorial Pacific and Bering Sea suggests that radiolytic H_2 is the primary microbial fuel in anoxic marine sediment older than a few Ma.

These H_2 results and the stoichiometry of water radiolysis [$2H_2O \rightarrow H_2 + H_2O_2$ (*17*)] have major implications for the electron-acceptor flux to subseafloor sedimentary ecosystems. First, in oxic sediment older than a few Ma, the flux of radiolytic oxidizing power greatly exceeds (by up to 86X) the net rate at which O_2 from the overlying ocean is reduced (**Figure 1.4A**). In short, our results suggest that gross respiration is dominantly powered by electron donors (H_2) *and* electron acceptors (H_2O_2 and its decomposition product O_2) from water radiolysis in all oxic marine sediment older than a few Ma.

Second, again given the stoichiometry of water radiolysis, our comparison of radiolytic H_2 production to net DIC production indicates that the flux of radiolytic H_2O_2 exceeds net organic-fueled respiration in relatively organic-rich anoxic marine sediment older than a few Ma (**Figure 1.4B**). Because H_2O_2 quickly decomposes to O_2 + H_2O (*4, 5*) or reacts with reduced chemicals to form other oxidized species [e.g., Fe(III), SO_4^{2-}], this result indicates that water radiolysis generates a significant continuous flux of electron acceptors in the nominally anoxic subseafloor sediment that blankets the continental margins and upwelling zones of the world ocean. This radiolytic oxidant flux may sustain cryptic redox processes at low rates in anoxic sediment, such as (i) NO_3^- reduction inferred from transcriptomic signatures (*29*) and (ii) SO_4^{2-} reduction inferred from radiotracer incubations (*30*) of samples taken from sediment deep beneath the last subseafloor occurrences of measurable dissolved NO_3^- and SO_4^{2-}. Because anoxic sediment is characterized by continuous *in situ* production of radiolytic H_2O_2 and its decomposition product O_2, this system is perhaps better considered as microoxic, at least on the timescales and distance scales over which radiolytic H_2O_2 and O_2 diffuse before they are reduced. This result is consistent with the majority of bacterial isolates from anoxic subseafloor sediment being facultative aerobes (*31*).

This study demonstrates the biological importance of abundant natural materials as catalysts of radiolytic chemical production. Discovery and quantification of this catalytic effect illuminates a previously cryptic source of bioavailable energy in subsurface environments. In doing so, it reshapes understanding of habitability on Earth and other worlds. Naturally catalyzed production of radiolytic chemicals is a primary source of electron donors and electron acceptors in marine sediment older than a few Ma throughout the ocean. It was presumably even more important for pre-photosynthetic life

on Early Earth. Where water permeates similarly catalytic material on other planets and moons, life may also be sustained by radiolytic H_2 and radiolytic oxidants.

Acknowledgments We thank the shipboard science parties and crew members of Ocean Drilling Program Leg 201, Integrated Ocean Drilling Program (IODP) Expeditions 323 and 329, RV Knorr expeditions 195-3 and 223, RV Endeavor expeditions 28, 32, and 534 and RV Marion Dufresne MONA expedition for samples and data. We thank the URI Marine Geological Samples Laboratory for samples. We thank the staff of the Rhode Island Nuclear Science Center (RINSC) for their advice and for providing materials and space for experiments. We thank Dennis Graham for his help and insight in the set up of radiation experiments. This project was funded by the National Aeronautics and Space Administration (grant NNX12AD65G); the US National Science Foundation (through grant NSF-OCE-1130735 and the Center for Deep Dark Energy Biosphere Investigations [grant NSF-OCE-0939564]); the U.S. Science Support Program associated with the IODP; and the Schlanger Ocean Drilling Fellowship Program. Portions of this material are based on work supported while R.W.M. was serving at the National Science Foundation. This is a contribution to the Deep Carbon Observatory (DCO). It is Center for Dark Energy Biosphere Investigations (C-DEBI) publication ###

References

1. Spinks, J. W. T., Woods, R. J. *An Introduction to Radiation Chemistry*, Wiley (1990).

2. Blair, C. C., D'Hondt, S., Spivack, A. J., Kingsley, R. H. Radiolytic hydrogen and microbial respiration in subsurface sediments. *Astrobiology* **7**, 951-970 (2007).

3. Sherwood Lollar, B., Onstott, T. C., Lacrampe-Couloume, G., Ballentine, C. J. The contribution of the Precambrian continental lithosphere to global H_2 production. *Nature* **516**, 379-382 (2014).

4. Navalon, S., Alvaro, M., & Garcia, H. Heterogeneous Fenton catalysts based on clays, silicas and zeolites. *Applied Catalysis B: Environmental* **99**, 1-26 (2010).

5. Abbot, J. and Brown, D.G. Kinetics of Iron-catalyzed decomposition of hydrogen peroxide in alkaline solution. *International journal of chemical kinetics* **22**, 963-974 (1990).

6. Morita, R. Y. Is H_2 the universal energy source for long-term survival?. Microbial ecology **38**, 307-320 (1999).

7. Lin, L. H., Hall, Lippmann-Pipke, J., Ward, J. A., Sherwood Lollar, B., DeFlaun, M., Rothmel, R., Moser, D., Gihring, T. M., Mislowack, B., Onstott, T. C. Radiolytic H_2 in continental crust: nuclear power for deep subsurface microbial communities. *Geochemistry, Geophysics, Geosystems* **6**, (2005).

8. Morita, R. Y., and ZoBell, C. E. Occurrence of bacteria in pelagic sediments collected during the Mid-Pacific Expedition. *Deep Sea Research* **3**, 66-73 (1955).

9. D'Hondt, S., Spivack, A. J., Pockalny, R., Ferdelman, T. G., Fischer, J. P., Kallmeyer, J., Abrams, L. J., Smith, d. C., Graham, D., Hasiuk, F., Schrum, H., Stancin, A. M. Subseafloor sedimentary life in the South Pacific Gyre. *Proceedings of the National Academy of Sciences* **106**, 11651-11656 (2009).

10. Lefticariu, L., Pratt, L. A., LaVerne, J. A., Schimmelmann, A. Anoxic pyrite oxidation by water radiolysis products - A potential source of biosustaining energy. *Earth and Planetary Science Letters* **292**, 57-67 (2010).

11. Bouquet, A., Glein, C. R., Wyrick, D., Waite, J. H. Alternative Energy: Production of H_2 by Radiolysis of Water in the Rocky Cores of Icy Bodies. *The Astrophysical Journal* **840**, L8 (2017).

12. Pastina, B., LaVerne, J. A. Effect of molecular hydrogen on hydrogen peroxide in water radiolysis. *The Journal of Physical Chemistry* **105**, 9316-9322 (2001).

13. Crumière, F., Vandenborre, J., Essehli, R., Blain, G., Barbet, J., Fattahi, M. LET Effects on the hydrogen production induced by the radiolysis of pure water. *Radiation Physics and Chemistry* **82**, 74-79 (2013).

14. LaVerne, J. A. Radiation chemistry of water with ceramic oxides. *Charged Particle and Photon Interactions with Matter: Recent Advances, Applications, and Interfaces*, CRC Press, 425-444 (2011).

15. Kumagai, Y., Kimura, A., Taguchi, M., Nagaishi, R., Yamagishi, I., Kimura, T. Hydrogen production in gamma radiolysis of the mixture of mordenite and seawater: Fukushima NPP Accident Related. *Journal of Nuclear Science and Technology* **50**, 130-138 (2013).

16. LaVerne, J. A., Tandon, L. H_2 production in the radiolysis of water on UO_2 and other oxides. *The Journal of Physical Chemistry* **107**, 13623-13628 (2003).

17. Pastina, B., LaVerne, J. A. Hydrogen peroxide production in the radiolysis of water with heavy ions. *The Journal of Physical* Chemistry **103**, 1592-1597 (1999).

18. R. Yamada, Y. Kumagai, R. Nagaishi, Effect of alumina on the enhancement of hydrogen production and the reduction of hydrogen peroxide in the γ-radiolysis of pure water and 0.4M H_2SO_4 aqueous solution. *International journal of hydrogen energy* **36**, 11646-11653 (2011).

19. Kumagai, Y. Decomposition of hydrogen peroxide by γ-ray irradiation in mixture of aqueous solution and Y-type zeolite. *Radiation Physics and Chemistry* **97**, 223-232 (2014).

20. Lin, S. S., Gurol, M. D. Catalytic decomposition of hydrogen peroxide on iron oxide: kinetics, mechanism, and implications. *Environmental Science & Technology* **32**, 1417-1423 (1998).

21. D'Hondt, S., Inagaki, F., Zarikian, C. A. and the Expedition 329 Scientists. *Proceedings of the Integrated Ocean Drilling Program*, Volume 329 (2011).

22. Khademian, M. and Imlay, J.A. Escherichia coli cytochrome c peroxidase is a respiratory oxidase that enables the use of hydrogen peroxide as a terminal electron acceptor. *Proceedings of the National Academy of Sciences* **114**, E6922-E6931 (2017).

23. Naval Oceanographic Office. Database description for surface sediment type. Stennis Space Center, Mississsippi: Acoustics Division (2003).

24. Martin, K. M., Wood, W. T., & Becker, J. J. A global prediction of seafloor sediment porosity using machine learning. Geophysical Research Letters **42** (2015).

25. Divins, D. L., Total Sediment Thickness of the World's Oceans & Marginal Seas, NOAA National Geophysical Data Center, Boulder, CO, (2003).

26. Behrenfeld, M. J. and Falkowski, P. G. Photosynthetic rates derived from satellite-based chlorophyll concentration. *Limnology and Oceanography* **42**, 1-20 (1997).

27. D'Hondt, S., Inagaki, F., Zarikian, C. A., Abrams, L. J., Dubois, N., Engelhardt, T., Evans, H., Ferdelman, T., Gribsholt, B., Harris, R. N., Hoppie, B. W., Hyun, J. H., Kallmeyer, J., Kim, J, Lynch, J. E., McKinley, C. C., Mitsunobu, S., Morono, Y., Murray, R. Y., Pockalny, R., Sauvage, J., Shimono, T., Shiraishi, F., Smith, D. C., Smith-Duque, C. E., Spivack, A. J., Steinsbu, B. O., Suzuki, Y., Szpak, M., Toffin, L., Uramoto, G., Yamaguchi, Y. T., Zhang, G. L., Zhang, X. H., Ziebis, W. Presence of oxygen and aerobic communities from sea floor to basement in deep-sea sediments. *Nature Geoscience* **8**, 299-304 (2015).

28. D'Hondt, S.L., Jørgensen, B.B., Miller, D.J., et al., 2003. *Proceedings of the Ocean Drilling Program, Initial Reports* Volume 201.

29. Orsi, W. D., Edgcomb, V. P., Christman, G. D., and Biddle, J. F. Gene expression in the deep biosphere. *Nature* **499**, 205-208 (2013).

30. Riedinger, N., Brunner, B., Krastel, S., Arnold, G.L., Wehrmann, L., Formolo, M.J., Beck, A., Bates, S.M., Henkel, S., Kasten, S. and Lyons, T.W. Sulfur cycling in an iron oxide-dominated, dynamic marine depositional system: The Argentine continental margin. *Frontiers in Earth Science* **5** (2017).

31. Batzke, A., Engelen, B., Sass, H., and Cypionka, H. Phylogenetic and physiological diversity of cultured deep-biosphere bacteria from equatorial Pacific Ocean and Peru Margin sediments. *Geomicrobiology Journal* **24**, 261-273 (2007).

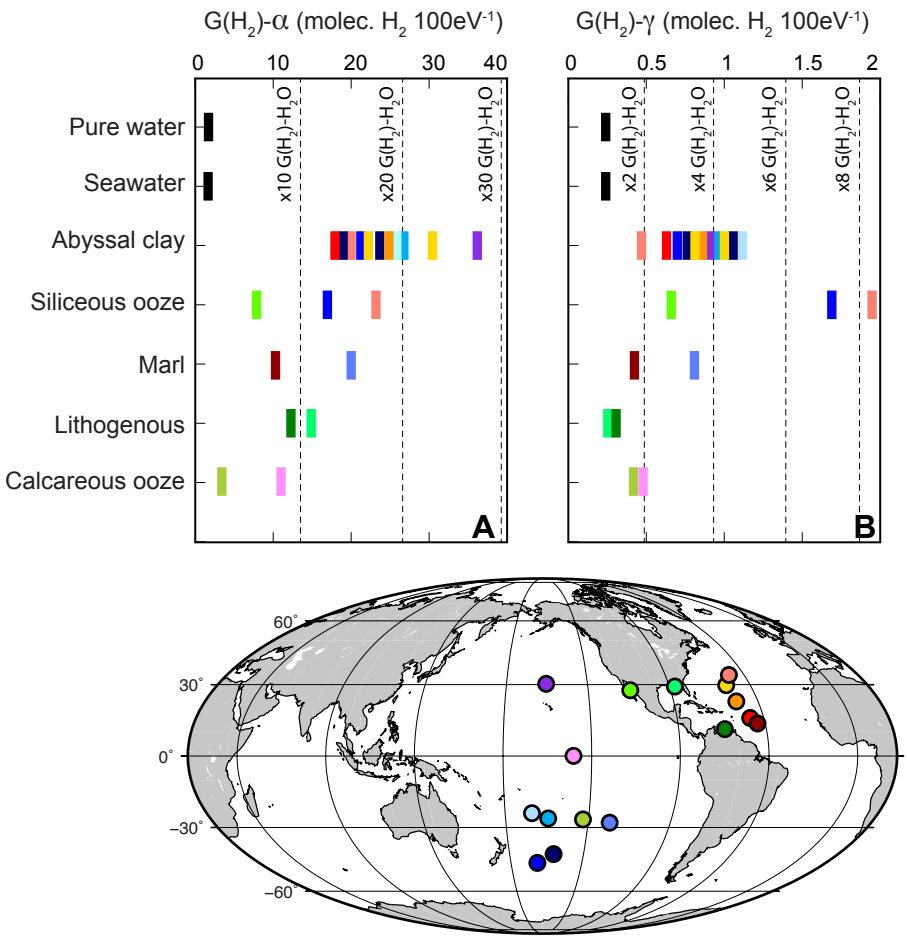

Figure 1.1. Radiolytic H_2 yields for α and γ radiation. A. Experimental H_2 yields from α irradiation (left) and γ irradiation (right). Vertical dashed lines represent multiples of production in pure water. **B.** Sample locations. Bar colors in A match sites of sample origin in B.

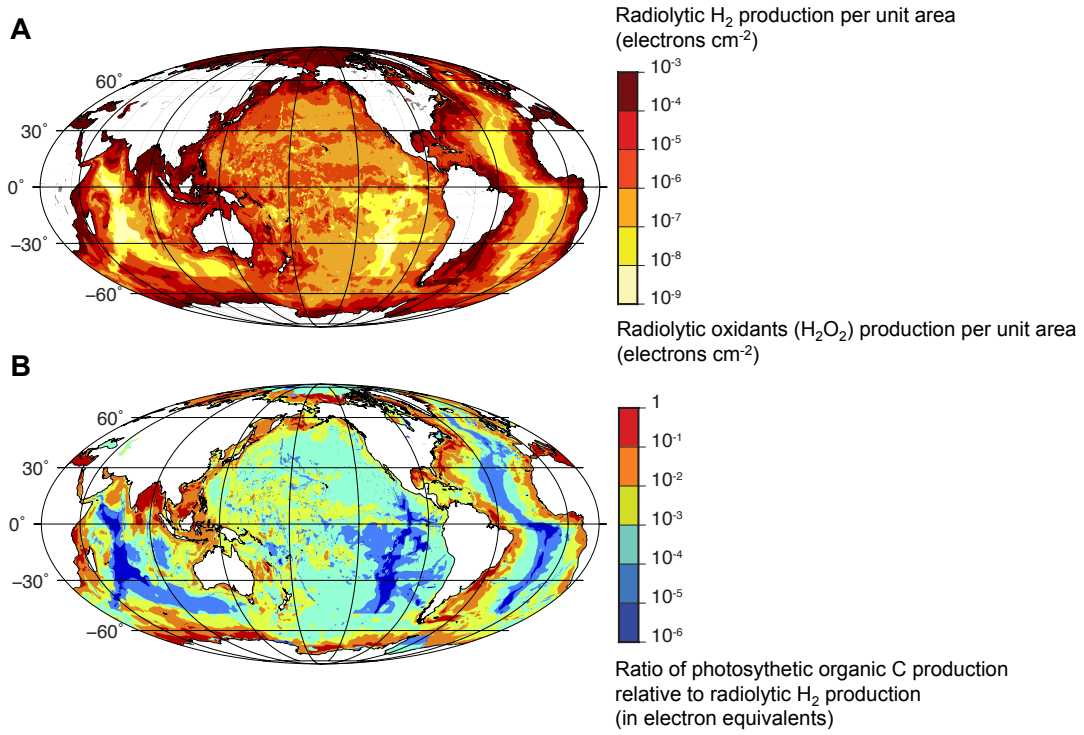

Figure 1.2. Global budget of radiolytic production in marine sediment. A. Global budget of radiolytic H_2 production and radiolytic H_2O_2 production expressed in electron equivalents (two electrons per H_2 molecule and two electrons per H_2O_2 molecule). Values are integrated over the thickness of the sediment column. **B.** Ratio of photosynthetic carbon production to radiolytic H_2 production on an electron-equivalent basis (four electrons per photosynthesized carbon atom).

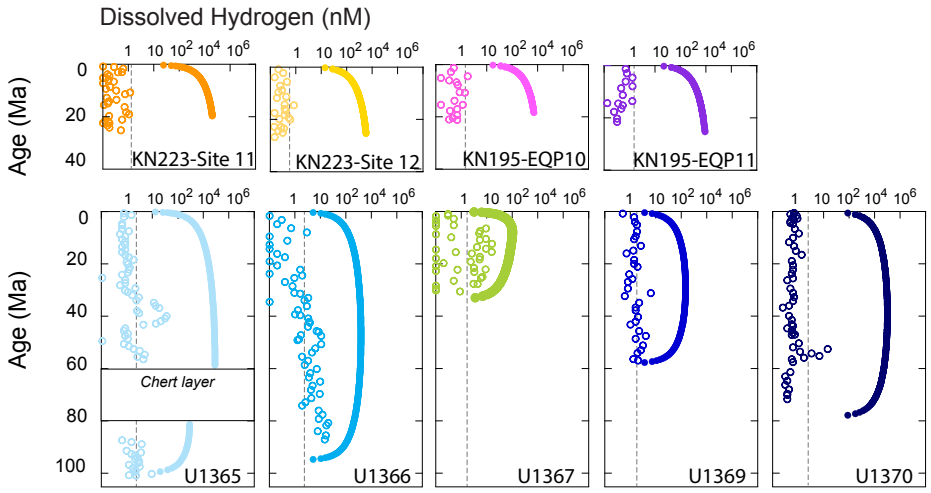

Figure 1.3. Measured and predicted H_2 concentration. Measured dissolved H_2 concentrations (o) as a function of sediment age at coring sites in the North Pacific (EQP 10 and 11), South Pacific (U1365-U1370) and North Atlantic (11 and 12). Solid circles (•) are H_2 concentrations expected from diffusion of radiolytic H_2 in the absence of *in situ* H_2 sinks. Gray vertical lines represent limits of detection for dissolved H_2 concentration measurements.

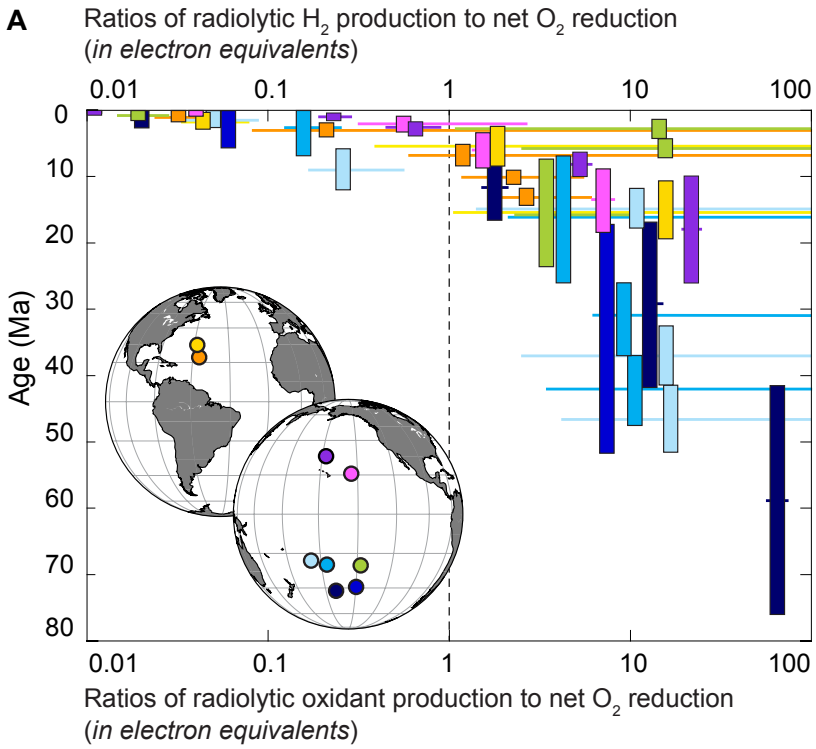

Figure 1.4.A. Contribution of radiolytic products in oxic sediment. Ratios of (i) radiolytic H_2 production to net O_2 reduction and (ii) radiolytic oxidant production to net O_2 reduction, (all in electron equivalents), plotted against sediment age for sites where sediment is oxic throughout all or most of the sediment column (SI). Horizontal lines represent first standard deviation of the ratio of radiolytic H_2 production to net O_2 reduction. Colors of bars and site locations match colors of site symbols in Figure 3.

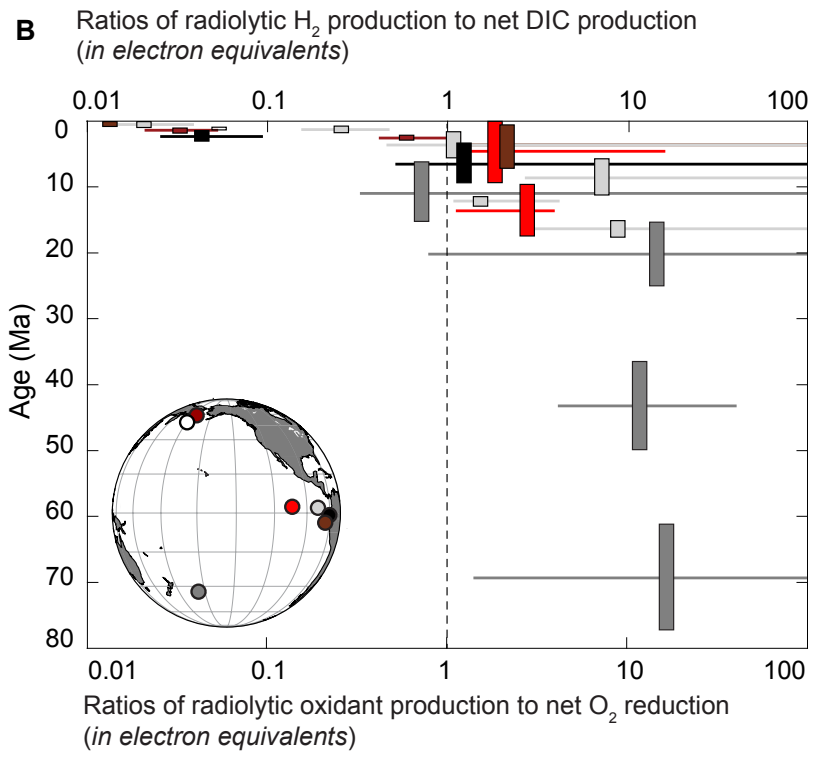

Figure 1.4.B. Contribution of radiolytic products in anoxic sediment. Ratios of (i) radiolytic H_2 production to net DIC production and (ii) radiolytic oxidant production to net DIC production (all in electron equivalents), in predominantly anoxic sediment. Horizontal lines represent first standard deviation of the ratio of radiolytic H_2 production to net DIC production. Colors of bars and site locations match colors of site symbols in Figure 3.

1.3. Supplemental information

1.3.1. Radiation experiment

We experimentally quantified radiolytic hydrogen (H_2) production for (i) pure water, (ii) seawater, and (iii) seawater-saturated sediment. We irradiated these materials with α and γ radiation for fixed time interval and then determined the concentrations of the resulting H_2. Sediment samples were slurried with natural seawater to achieve a slurry porosity (φ) of ~0.83. The seawater source is described below. To avoid microbiological uptake of radiolytic H_2 during the course of the experiment seawater and marine sediment slurries were pre-treated with $HgCl_2$ [0.05% solution] or NaN_3 [0.1%wt/vol]). To ensure that addition of these chemicals did not impact radiolytic H_2 yields, irradiation experiments with pure water plus $HgCl_2$ or NaN_3 were also conducted. $HgCl_2$ or NaN_3 addition had no statistically significant impact on H_2 yields (1,2).

Experimental samples were irradiated in 250mL borosilicate vials. A solid-angle ^{137}Cs source (beam energy of 0.67 MeV) was used in the γ-irradiation experiments at the Rhode Island Nuclear Science Center (RINSC). The calculated dose rate for sediment slurries was 2.19E-02 Gy/h accounting for the (i) source activity, (ii) distance between the source and the samples, (iii) samples vial geometry and attenuation coefficient of γ-radiation through air, borosilicate and sediment slurry. ^{210}Po (5.3 MeV $decay^{-1}$) plated silver strips with a total activity of 250 μCi were used in the α-irradiation experiments. Total absorbed doses were 4 Gy and 3 kGy for γ-irradiation and α-irradiation experiments, respectively.

The settling time of sediment grains in the slurries (one week) was slow compared to the time span of each experiment (10s of minutes for α-experiments, hours to days for γ

experiments). Therefore, it is assumed that the solution was homogenous during the course of each experiment.

Post-radiation H_2 concentrations were measured by quantitative headspace analysis via gas chromatography. For headspace analysis, 30 mL of N_2 gas headspace was first injected into the sample vial. To avoid over-pressurization of the sample during headspace injection, an equivalent amount of water was allowed to escape from the vial through a separate needle. Then the vials were vigorously shaken for 5 min to concentrate the H_2 in the headspace. Finally, a 500-μL-headspace subsample was injected into a reduced gas analyzer (Peak Performer 1, PP1). The reduced gas analyzer was calibrated using a 1077 ppmv H_2 gas standard (Scott-Marrin, Inc.) and a gas mixer. A gas mixer was used to dilute the H_2 standard with N_2 gas to obtain various H_2 concentrations and produce a five-point calibrations curve (at 0.7, 2, 5, 20 and 45 ppm H_2). H_2 concentrations of procedural blank samples consisting of sample vials filled with non-irradiated 18-MΩ water (distilled and deionized) were also determined. The H_2 concentration detection limit obtained using this protocol was 0.8-1 nM H_2. Error in gas measurements was less than 5%.

To calculate H_2 concentration as a function of total absorbed dose each sample was exposed to radiation over a time interval during which H_2 was measured multiple times. This was done in duplicate. We verified the reliability of our experimental protocols for both α and γ irradiation experiments, with pure-water experiments, which had yields indistinguishable from those previously reported in the literature (1,2,3).

1.3.2. Sample selection and experimentally quantified radiolytic H_2 yields, $G(H_2)$

Millipore Milli-Q UV system water was used for our pure-water experiments. For seawater experiments, bottom water collected in the Hudson Canyon (water depth, 2136 m)

during Endeavor expedition EN534 was used. Salinity of North Atlantic bottom water in the vicinity of the Hudson Canyon (salinity 34.96gms/kg) is very close to that of mean open-ocean bottom water (salinity 34.70 gms/kg) [4,5].

The 20 experimental sediment samples were collected by scientific coring expeditions in three ocean basins [expedition KN223 to the North Atlantic, expedition KN195-R to the Equatorial and North Pacific, International Ocean Discovery Program (IODP) expedition 329 to the South Pacific Gyre (6), MONA expedition to the Guaymas Basin (7), expedition EN32 to the Gulf of Mexico and expedition EN28 to the Venezuela Basin (8)]. To capture the full scope of sediment types present in the global ocean, we selected samples typical of 5 common sediment types [abyssal clay (11 samples), nannofossil-bearing clay or marl (2 samples), clay-bearing diatom ooze (3 samples), nannofossil ooze (2 samples) and lithogenic sediment (2 samples)]. The complete location and lithological details for each sample are given in **Supp. Table 1** and **Supp. Figure 1**.

Energy normalized radiolytic H_2 yields are commonly expressed as $G(H_2)$-values (molecules H_2 per 100eV absorbed) for a given radiation type (9). As shown in **Supp. Figure 2**, for all irradiated samples (pure water, seawater, and marine sediment slurries) H_2 production increased linearly with absorbed α- and γ-ray-dose. We calculated $G(H_2)$-values for each sample and radiation type (α or γ) as the slope of the least-square regression line of total adsorbed dose versus radiolytic H_2 concentration (**Supp. Figure 2**). The results are reproducible and the error on the yields is less than 10% for each sample. $G(H_2)$-values for each sample and radiation type (α or γ) are reported in **Supp. Table 2**.

1.3.3. Subseafloor radiolytic H_2 production rate

We calculated subseafloor radiolytic H_2 production rates at nine oxic sediment sites across the North and South Pacific and the North Atlantic (**Supp. Figure 4**, see **Supp. Figure 3** for site location). This calculation is based on sedimentary radiolysis model of Blair *et al.* (10) and utilizes (i) our experimentally derived $G(H_2)$ values, (ii) measured bulk sedimentary U, Th and K abundances, and (iii) porosity and grain density,.

The γ-radiation dosage in subseafloor sediment is three orders of magnitude lower than the dosage used in our radiation experiments to determine γ-$G(H_2)$ values. Because the $G(H_2)$ for pure water in our γ-irradiation experiment [dose rate = 3.30E-02 Gy h^{-1}] is statistically indistinguishable from previously published $G(H_2)$ values at much higher dose rates [ca. 1 kGy h^{-1} (2)] we infer that the γ-irradiation $G(H_2)$ value is constant with dose rate over five orders of magnitude. Therefore we use our experimentally determined $G(H_2)$ for the low radiation dose rate found in the subseafloor. Because the $G(H_2)$ of β irradiation has not been experimentally determined for water-saturated materials, it was assumed that the $G(H_2)$ of β radiation matches the $G(H_2)$ of γ radiation for the same sediment types. In pure water, their $G(H_2)$ values differ by only 17% (9). Because β radiation, on average, contributes only 11% of the total radiolytic H_2 production from the U, Th series and K decay in deep-sea sediment, these estimates of total H_2 production differ by only 2% relative to estimates where the $G(H_2)$ of β radiation is assumed equal to that for pure water or for α radiation of the same sediment types.

To calculate downhole subseafloor H_2 production rates at nine sites across the global ocean U, Th and K concentrations were measured in (i) 187 sediment samples from seven IODP Expedition 329 sites (U1365, U1366, U1367, U1368, U1369, U1370 and U1371) [6]

and (ii) 40 samples from two deep-ocean sites cored by the KN223 expedition (KN223 Site 11 and Site 12) [11]. Total U and Th (ppm) and K_2O (wt%) for these sites are reported in the EarthChem SedDB data repository. DOI's: (U) 10.1594/IEDA/100606; (Th) 10.1594/IEDA/100605; (K) 10.1594/IEDA/100604.

We measured U, Th and K abundances using standard atomic emission and mass spectrometry techniques (i.e. ICP-ES and ICP-MS) in the Analytical Geochemistry Facilities at Boston University. Sample preparation, analytical protocol, and data are reported in Dunlea *et al.* (12). The precision for each element is ~2% of the measured value, based on three separate digestions of a homogenized in-house standard of deep-sea sediment.

To calculate subseafloor H_2 production rates for North Pacific coring Sites EQP 10 and EQP 11, radioactive element content data from Kyte *et al.* (1993), who measured chemical concentrations at high resolution in bulk sediment from site LL44-GPC3 was used. Site EQP11 was cored at the same location as Site LL44-GPC3 [13].

1.3.4. Global budget of radiolytic H_2 production in marine sediment

We calculate global radiolytic H_2 production in marine sediment by using the same calculation protocol described earlier (i.e. model of water radiolysis for fine-grained sedimentary environments, [10]). This calculation spatially integrates modeled sedimentary porewater radiolysis rates which are based on (ii) our experimentally constrained radiolytic H_2 yields for the principal marine sediment types, (iii) measured radioactive element content of sediment cores in three ocean basins (North Atlantic [11], North [13] and South Pacific [6,12]), and global distributions of (iii) seafloor lithology (14), (iv) sediment porosity (15), and (v) sediment thickness (16,17).

To perform a global calculation of radiolytic H_2 production the geographic database of global surface sediment types was subdivided (14,18) into five lithology categories: abyssal

clay, calcareous ooze, siliceous ooze, marl, lithogenous and "other" (**Supp. Figure 5**). The "other" category was designed to group all areas of the seafloor that were not described in the database. These includes the higher latitudes as the seafloor lithology database extends from 750°N to 50°S (14) and some discrete areas located along the continental margins (e.g. Mediterranean Sea, Timor Sea, South China Sea, **Supp. Figure 5**). To complete the database for high latitudes we added an opal belt (siliceous ooze) in the Southern Ocean between 57°S and 66°S (18,19). The geographic extent of this opal belt was extracted from DeMaster (2002) and Dutkiewicz *et al.* (2015). The remaining areas of the seafloor extending from from 50°S to 57°S, 66°S to 90°S and the Arctic Ocean seafloor were described as mostly composed of lithogenous material following spot checking in the Southern Ocean (ODP: Site 695 [20], Site 694 [21], Site 1165 [22], Site 739 [23]), in the Bearing Sea and Arctic Ocean (International Ocean Discovery Program (IODP): Site U1343 and U1345 [24] Site M0002 [25], ODP: Site 910 [26], Site 645 [27]) and between 50°S and 57°S (Deep Sea Drilling Project (DSDP): site 326 [28], Ocean Drilling Program (ODP): Site 698 [29], Site 1138 [30], Site 1121 [31]) and from Dutkiewicz *et al.* (2015).

After spot-confirmation of the seafloor lithologies found in the areas grouped as "other" between 70°N to 50°S and based on the interpolated seafloor lithology map derived by Dutkiewicz *et al.* (2015) these areas are taken to be mostly composed of detrital clays with some fraction of biogenic material. Lithologic descriptions of sediment cores from the DSDP: Site 344 [32], Site 267 [33], Site 322 [34]; ODP: Site 642 [35], Site 767 [36], Site 963 [37], and IODP: Site U1355 [38], were used to spot confirm the seafloor sediment type in these areas.

In our global calculation of radiolytic H_2 production in marine sediment it is assumed the assigned seafloor sediment type is invariant with depth, except for the North and South

Atlantic. Because of the relative young age of the Atlantic Ocean basin (180 Ma) most of the sediment consists of 30-90% biogenic carbonate content and detrital clay (39). This is apparent when spot checking discrete locations in the North and South Atlantic (ODP: Site 1063 (40), Site 951 (41), Site 925 (42), Site 662 (43), IODP: Site U1403 (44), Site U1312 (45) Therefore, regions in the Atlantic Ocean described as abyssal clay in the surface sediment type database (14) were characterized as marl in our calculations (**Supp. Figure 5**).

To perform the global calculation, each lithology type is assigned a characteristic set of $G(H_2)$-values (α, β-and-γ radiation), radioactive element content (sedimentary U, Th and K concentration) and grain density (**Supp. Table 3**). These set of variables were determined as follows,

$G(H_2)$-α,β-&-γ

Radiolytic yields for the main seafloor lithologies were obtained by averaging experimentally derived yields for the respective lithologies (**Supp. Table 2**). It is assumed that $G(H_2)$-β values equal $G(H_2)$-γ values.

Radioactive element content

Measured U, Th and K concentrations from sites in North Atlantic [11], North [13] and South Pacific [6,12] were grouped based on described sediment type of the samples (i.e. abyssal clay, siliceous ooze, calcareous ooze and marl). The radioactive elements content were averaged per lithology and the lithology-specific averaged values were used as input parameters for the radiolysis model. The averaged U, Th, and K concentration values are consistent with data reported in Li and Schoonmaker (2003) for the characteristic U, Th and K content found in abyssal clay and calcareous ooze. For lithogenous sediment, characteristic U, Th, and K concentration values for upper continental crust as reported in Li and Schoonmaker (2003) were used (46).

Grain density

Characteristic grain density values for calcite, quartz, terrigenous clay and opal rich sediment were extracted from (47) and assigned to calcareous ooze, lithogenous sediment, abyssal clay, and siliceous ooze respectively (47). These values were confirmed with grain density data measured in South Pacific Gyre sites (6).

Generated input maps to run the radiolysis model

Global maps of seafloor U (**Supp. Figure 6**), Th (**Supp. Figure 7**) and K (**Supp. Figure 8**) sediment content, grain density (**Supp. Figure 9**), $G(H_2)$-α values (**Supp. Figure 10**) and $G(H_2)$-γ-and-β (**Supp. Figure 11**) required as inputs in the radiolysis model were generated by assigning each grid cell in our compiled seafloor lithology map (**Supp. Figure 5**) its lithology-specific set of input variable (**Supp. Table 3**) . Because the sediment composition of the seafloor areas labeled as "other" in **Supp. Figure 5** are similar in composition to lithogenous sediment they are assigned the same "lithogenous sediment" set of input parameters to grid cells located in the "other" category. Because a constant lithology was assumed with depth it was also assumed that U, Th, and K content, grain density and $G(H_2)$-values are constant with depth.

Porosity

For global porosity, a seafloor porosity data set by Martin *et al.* (2015) was used [**Supp. Figure 12**]. Sediment compaction with depth was accounted for by using sediment compaction length scales representative for continental shelf ($c_0 = .5x10^{-3}$), continental margin ($c_0 = 1.7x10^{-3}$) and abyssal sedimentary environments ($c_0 = .85x10^{-3}$) (49) following methods found in LaRowe *et al.* (2017). Once the porosity was 0.1 %, the depth integration was halted.

Sediment Thickness

To calculate global subseafloor radiolytic H_2 production, the described global maps (**Supp. Figure 3 through 12**) were used (10). Global, depth integrated radiolytic H_2 production was calculated by integrating the seafloor production rates over sediment thickness (**Supp. Figure 13**) in one meter depth intervals. (Figure 2A in Main Text). Sediment thickness was taken from Whittaker et al. (2013) infilled with Laske and Masters (1997) where needed.

1.3.5. Comparison of photosynthetic organic carbon production relative to radiolytic H_2 production

We used monthly net primary production data for 2016 to create a yearly carbon fixation map (in molC/cm^2/yr) (**Supp. Figure 14**). This data was extracted from the standard Products of The Ocean Productivity (http://www.science.oregonstate.edu/ocean.productivity/index.php) and were based on the original description of the Vertically Generalized Production Model (VGPM) [52], MODIS surface chlorophyll concentrations (Chl_{sat}), MODIS 4-micron sea surface temperature data (SST4), and MODIS cloud-corrected incident daily photosynthetically active radiation (PAR). Euphotic depths were calculated from Chl_{sat} following Morel and Berthon (1989).

The rate of photosynthetic carbon fixation (in molC/cm^2/yr, **Supp. Figure 14**) to depth integrated radiolytic H_2 production (in molH_2/cm^2/yr, **Figure 2A** in Main Text) are compared, by converting both H_2 and organic carbon production rates to electron equivalents transferred per mol H_2 and mol carbon (CH_2O) oxidized, respectively. This was done by accounting for two electrons transferred per mol H_2 ($H_2 + ½O_2 \rightarrow H_2O$) and 4 electrons per mol C ($CH_2O + O_2 \rightarrow CO_2 + H_2O$) oxidized, respectively. The relative

importance of these electron donors is calculated by dividing the production rates photosynthetic organic carbon by the production rate of radiolytic H_2 in terms of electron equivalence per unit area (**Supp. Figure 14 and Figure 1B in the Main text).** In **Figure 2B** in the Main Text this ratio is mapped for the whole ocean.

1.3.6. Dissolved H_2 concentrations

Dissolved H_2 concentrations for South Pacific sites and measurement protocols are described in reference (6). Dissolved H_2 concentrations for the North Atlantic (KN223-Site 11 and 12) and North Pacific (EQP 10 and EQP11) sites were determined using the same protocol and are accessible on SedDB. Measured dissolved H_2 concentrations as a function of sediment age at coring sites in the North Pacific, South Pacific and North Atlantic are displayed in Figure **Supp. Figure 15** as open circles (**o**). The detection limit for dissolved H_2 concentration measurements ranged between 1 and 5 nM H_2 depending on site and is displayed as gray vertical lines on **Supp. Figure 15**. Predicted *in situ* H_2 concentrations were calculated based on diffusion-reaction calculations in the absence of H_2-consuming reactions and in the presence of diffusive loss of H_2 to both the overlying ocean and underlying basement aquifer. Predicted H_2 concentrations from diffusion are represented as solid circles (•) on **Supp. Figure 15**.

1.3.7. Gibbs Energy of the knallgas reaction

Where dissolved H_2 concentrations are above the detection limit (1-5 nM H_2) at IODP Expedition 329 sites in the South Pacific [**Supp. Figure 16**] (6), we quantified the *in situ* Gibbs energy of (ΔG_r) of the *knallgas* reaction ($H_2 + ½O_2 \rightarrow H_2O$). *In situ* ΔG_r values depend on pressure (P), temperature (T), ionic strength and chemical concentrations, all of which are explicitly accounted for in our calculations:

$\Delta G_r = \Delta G°_r(T,P) + 2.3\ RT\ log_{10}Q$

Where:

ΔG_r: *in situ* Gibbs energy of reaction (kJ $molH_2^{-1}$)

$\Delta G°_r(T,P)$: Gibbs energy of reaction under *in situ* T and P conditions (kJ $molH_2^{-1}$)

R: gas constant (8.314 kJ mol^{-1} K^{-1})

Q: activity quotient of compounds involved in the reaction

We used the measured composition of the sedimentary pore fluid to determine values of Q. For a more complete overview of *in situ* Gibbs energy-of-reaction calculations in subseafloor sediment, see Wang *et al.* (54).

1.3.8. Sediment age determination

We used the mean sedimentation rate for each site (aerobic sites: U1365, U1366, U1367, U1369, U1370, EQP 10, EQP 9, Site 11, Site 12; anaerobic sites: U1345, U1343, U1371, 1225, 1226, 1230, 1231 **Supp. Figure 3**) to convert sediment depth (in meters below seafloor) to sediment age (in millions of years, Ma). This approach implicitly assumes a constant sedimentation rate for each site. Mean sedimentation rate is calculated by dividing the depth of the sediment column by the basement age (**Supp. Table 4**) for South Pacific sites (U1365, U1366, U1367, U1369, U1370 and U1371), North Atlantic sites (KN223-Site 11, KN223-Site 12) and North Pacific sites (EQP10 and EQP11). Sediment thicknesses were determined from acoustic basement reflection data. Basement ages are from Muller et al. (2008, 55). For Equatorial Pacific sites (1225 and 1226), Peru trench Site 1230 and Peru Basin Site 1231 sediment accumulation rates were determined using ^{14}C chronology (56,57). For Bearing Sea (U1343 and U1345) sedimentation rates inferred from geochronologic and biostratographic methods were used (24).

1.3.9. Subseafloor radiolytic oxidants production rates and comparison with net DIC production rate at anoxic sites

Radiolytic H_2O_2 (and its degradation product O_2) production rates were calculated at six sites in anaerobic sedimentary environments (see **Supp. Figure 3** for site locations). Radiolytic oxidant production rates were derived from radiolytic H_2 production rates calculated as described above in previous section. We inferred oxidants production rates according to the stoichoiometric production of oxidants in the radiolysis of water:

Water radiolysis: $2H_2O \rightarrow H_2 + H_2O_2$

Decomposition of H_2O_2: $2H_2O_2 \rightarrow 2H_2O + O_2$

The obtained radiolytic oxidant production rates were further compared to net production of dissolved Inorganic Carbon (DIC) at these sites. Downhole DIC concentrations were obtained from the ODP and IODP related site reports (sites U12343, U1345, U1371, 1225, 1226, 1230, and 1231 [24,6,56]). Based on the measured downhole DIC concentration profiles vertical distributions of net DIC production rates were quantified using the MatLab program and numerical procedures of Guizhi *et al.* (2008). Details of the calculation protocol are described in the supplementary information of D'Hondt *et al.* (2015). Calculated downhole DIC reaction rates and the first standard deviation for the seven sites are given in **Supp. Table 4.**

In order to facilitate comparisons of radiolytic oxidants (O_2-H_2O_2) production rates to net DIC production rates, rates were converted on the basis of electron equivalents transferred:

1. $H_2 + ½O_2 \rightarrow H_2O$ (2 electrons transferred per mol H_2 oxidized)

2. Organic fueled respiration: $CH_2O \rightarrow CO_2$. The electrons transferred during the oxidation of organic matter are quantified based on the Redfield ratio of organic matter (106 C/16

N/1 P/-170 O_2, 60). Four electrons are transferred per O_2 reduced, eight electrons are transferred per ammonium oxidized. Therefore based on the redfield ratio we calculate: 106 (electrons $(e\text{-})^-$ transferred per mol C oxidized) + 16 (8 e^-/mol NH_3) = 170(4 e^-/mol O_2). Based on above calculation we calculate that 5.2 electrons are transferred per mol DIC produced.

References

1. Pastina, B., LaVerne, J.A. Effect of molecular hydrogen on hydrogen peroxide in water radiolysis. *The Journal of Physical Chemistry* **105**, 9316-9322 (2001).
2. Crumière, F., Vandenborre, J., Essehli, R., Blain, G., Barbet, J., Fattahi, M. LET Effects on the hydrogen production induced by the radiolysis of pure water. *Radiation Physics and Chemistry* **82**, 74-79 (2013).
3. Essehli, R., Crumière, F., Blain, G., Vandenborre, J., Pottier, F., Grambow, B., Fattahi, M., Mostafavi, M. H_2 production by γ and He ions water radiolysis, effect of presence TiO_2 nanoparticles. *International journal of hydrogen energy* **36**, 14342-14348 (2011).
4. Talley, L. D. Hydrographic Atlas of the World Ocean Circulation Experiment (WOCE). Volume 2: Pacific Ocean (eds. M. Sparrow, P. Chapman and J. Gould), International WOCE Project Office, Southampton, U.K., 2007).
5. Koltermann, K. P., Gouretski, V. V., Jancke, K. Hydrographic Atlas of the World Ocean Circulation Experiment (WOCE). Volume 3: Atlantic Ocean (eds. M. Sparrow, P. Chapman and J. Gould). International WOCE Project Office, Southampton, UK, 2011).
6. D'Hondt, S., Inagaki, F., Zarikian, C. A. and the Expedition 329 Scientists, *Proceedings of the Integrated Ocean Drilling Program* Volume **329** (2011).

7. Cheshire, H., Thurow, J. High-resolution migration history of the Subtropical High/Trade Wind system of the northeastern Pacific during the last~ 55 years: Implications for glacial atmospheric reorganization. *Paleoceanography* **28**, 319-333 (2013).
8. Wright, A. Sediment Distribution and depositiona processes operating in the Lesser Antilles Intraoceanic Island-Arc, Eastern Carrabean. *Initial reports of the Deep Sea Drilling Project* **78**, 301-324 (1984).
9. Spinks, J. W. T., Woods, R. J. An Introduction to Radiation Chemistry (Wiley, 1990).
10. Blair, C. C., D'Hondt, S., Spivack, A. J., Kingsley, R. H. Radiolytic hydrogen and microbial respiration in subsurface sediments. *Astrobiology* **7**, 951-970 (2007).
11. Murray and R/V Knorr Cruise KN223 scientists, Cruise Report (2014).
12. Dunlea, A. G., Murray, R. W., Sauvage, J., Spivack, A. J., Harris, R. N., D'Hondt, S. Dust, volcanic ash, and the evolution of the South Pacific Gyre through the Cenozoic. *Paleoceanography* **30**, 1078-1099 (2015).
13. Kyte, F. T., Leinen, M., Heath, G. R., & Zhou, L. Cenozoic sedimentation history of the central North Pacific: Inferences from the elemental geochemistry of core LL44-GPC3. *Geochimica et Cosmochimica Acta* **57**, 1719-1740 (1993).
14. Naval Oceanographic Office. Database description for surface sediment type. Stennis Space Center, Mississsippi: Acoustics Division (2003).
15. Martin, K. M., Wood, W. T., & Becker, J. J. A global prediction of seafloor sediment porosity using machine learning. *Geophysical Research Letters* **42** (2015).
16. Divins, D. L., Total Sediment Thickness of the World's Oceans & Marginal Seas, NOAA National Geophysical Data Center, Boulder, CO, (2003).
17. Masters, G., Laske, G. On bias in surface wave and free oscillation attenuation measurements. *EOS* Trans.-Am. Geophys. Union, 78, F485 (1997).

18. Dutkiewicz, A., Müller, R. D., O'Callaghan, S., Jónasson, H. Census of seafloor sediments in the world's ocean. *Geology* **43**, 795-798 (2015).

19. DeMaster, D. J. The accumulation and cycling of biogenic silica in the Southern Ocean: revisiting the marine silica budget. *Deep Sea Research Part II: Topical Studies in Oceanography* **49**, 3155-3167 (2002).

20. Shipboard Scientific Party. Site 695. In Barker, P.E, Kennett, J.P., et al., Proc. ODP, Init. Repts., 113: College Station, TX (Ocean Drilling Program), 527–606 (1988).

21. Shipboard Scientific Party. Site 694. In Barker, P.E, Kennett, J.P., et al., Proc. ODP, Init. Repts., 113: College Station, TX (Ocean Drilling Program), 449–525 (1988).

22. Shipboard Scientific Party. Site 1165. In O'Brien, P.E., Cooper, A.K., Richter, C., et al., Proc. ODP, Init. Repts., 188: College Station, TX (Ocean Drilling Program), 1–191 (2001).

23. Shipboard Scientific Party. Site 739. In Barron, J., Larsen, B., et al., Proc. ODP, Init. Repts., 119: College Station, TX (Ocean Drilling Program), 289–344 (1989).

24. Takahashi, K., Ravelo, A.C., Alvarez Zarikian, C.A., and the Expedition 323 Scientists Proceedings of the Integrated Ocean Drilling Program, Volume 323 (2011).

25. Expedition 302 Scientists, 2006. Sites M0001–M0004. In Backman, J., Moran, K., McInroy, D.B., Mayer, L.A., and the Expedition 302 Scientists. Proc. IODP, 302: Edinburgh (Integrated Ocean Drilling Program Management International, Inc), (2006).

26. Shipboard Scientific Party. Site 910. In Myhre, A.M., Thiede, J., Firth, J.V., et al., Proc. ODP, Init. Repts., 151: College Station, TX (Ocean Drilling Program), 221–270 (1995).

27. Shipboard Scientific Party. Site 645. In Srivastava, S.P., Arthur, M., Clement, B., et al., Proc. ODP, Init. Repts., 105: College Station, TX (Ocean Drilling Program), 61–418 (1987).

28. Peter Barker, Ian W.D. Dalziel, Menno G. Dinkelman, David H. Elliot, Andrew M. Gombos, Jr., Alberto Lonardi, George Plafker, John Tarney, Robert W. Thompson, R.C. Tjalsma, Christopher C. von der Borch, and Sherwood W. Wise, Jr. – site 326.
29. Shipboard Scientific Party. Site 698. In Ciesielski, P.F., Kristoffersen, Y., et al., Proc. ODP, Init. Repts., 114: College Station, TX (Ocean Drilling Program), 87–150 (1988).
30. Shipboard Scientific Party. Site 1138. In Coffin, M.F., Frey, F.A., Wallace, P.J., et al., Proc. ODP, Init. Repts., 183: College Station, TX (Ocean Drilling Program), 1–205 (2000).
31. Carter, R.M., McCave, I.N., Richter, C., Carter, L., et al., *Proceedings of the Ocean Drilling Program, Initial Reports* Volume 181 (1999).
32. Deep Sea Drilling Project Volume 344
33. Deep Sea Drilling Project Volume 267
34. Deep Sea Drilling Project Volume 322
35. Eldholm, O., Thiede, J., Taylor, E., et al. *Proceedings of the Ocean Drilling Program, Initial Reports,* Vol. 104: College Station, TX Ocean Drilling Program (1987).
36. Rangin, C., Silver, E.A., von Breymann, M.T., et al. *Proceedings of the Ocean Drilling Program, Initial Reports,* Vol. 124: College Station, TX Ocean Drilling Program (1990).
37. Emeis, K.-C, Robertson, A.H.F., Richter, C, et al. *Proceedings of the Ocean Drilling Program, Initial Reports,* Vol. 160. College Station, TX Ocean Drilling Program (1996).
38. Escutia, C., Brinkhuis, H., Klaus, A., and the Expedition 318 Scientists. *Proceedings of the Integrated Ocean Drilling Program*, Volume 318. College Station, TX Ocean Drilling Program (2011).
39. Schulz, Horst D., and Matthias Zabel. Marine Geochemistry. Berlin: Springer, 2006.

40. Shipboard Scientific Party. Bermuda Rise and Sohm Abyssal Plain, Sites 1063 and 1064. In Keigwin, L.D., Rio, D., Acton, G.D., et al., Proc. ODP, Init. Repts., 172: College Station, TX (Ocean Drilling Program), 251–308 (1998).
41. Schmincke, H.-U., Weaver, P.P.E., Firth, J.V ., et al., Proceedings of the Ocean Drilling Program, Initial Reports, Vol. 157 (1995).
42. Shipboard Scientific Party. Site 925. In Curry, W.B., Shackleton, N.J., Richter, C., et al., Proc. ODP, Init. Repts., 154: College Station, TX (Ocean Drilling Program), 55–152 (1995).
43. Shipboard Scientific Party. Site 662. In Ruddiman, W., Sarnthein, M., Baldauf, J., et al., Proc. ODP, Init. Repts., 108: College Station, TX (Ocean Drilling Program), 487–556 (1988).
44. Norris, R.D., Wilson, P.A., Blum, P., and the Expedition 342 Scientists Proceedings of the Integrated Ocean Drilling Program, Volume 342
45. Channell, J.E.T., Kanamatsu, T., Sato, T., Stein, R., Alvarez Zarikian, C.A., Malone, M.J., and the Expedition 303/306 Scientists Proceedings of the Integrated Ocean Drilling Program, Volume 303/306.
46. Li, Y.H. and Schoonmaker, J.E. Chemical composition and mineralogy of marine sediments (pp. 1-35) (2003).
47. Pälike, H., Lyle, M., Nishi, H., Raffi, I., Gamage, K., Klaus, A., and the Expedition 320/321 Scientists. *Proceedings of the Integrated Ocean Drilling Program*, Volume 320/321 (2010).
48. LaRowe, Douglas E., Ewa Burwicz, Sandra Arndt, Andrew W. Dale, and Jan P. Amend. Temperature and volume of global marine sediments. *Geology* **45**, 275-278 (2017).

49. Hantschel, Thomas, and Armin I. Kauerauf. Fundamentals of basin and petroleum systems modeling. Springer Science & Business Media, (2009).

50. Whittaker, J., Goncharov, A., Williams, S. R., Müller, D., Leitchenkov, G. Global sediment thickness dataset updated for the Australian-Antarctic Southern Ocean. *Geochemistry, Geophysics, Geosystems* (2013).

51. Laske G. and G. Masters. A Global Digital Map of Sediment Thickness, *EOS Trans. AGU* **78**, F483 (1997).

52. Behrenfeld, M. J, Falkowski P. G. Photosynthetic rates derived from satellite-based chlorophyll concentration. *Limnology and Oceanography* **42**, 1-20 (1997).

53. Morel, A, Berthon, J. F. Surface pigments, algal biomass profiles, and potential production of the euphotic layer: Relationships reinvestigated in view of remote-sensing applications. Limnology and Oceanography 34, 1545-1562 (1989).

54. Guizhi, W., Spivack, A. J., D'Hondt, S. Gibbs energies of reaction and microbial mutualism in anaerobic deep subseafloor sediments of ODP Site 1226. *Geochimica et Cosmochimica Acta* **74**, 3938-3947 (2010).

55. Muller, R.D., Sdrolias, M., Gaina, C., Roest, W. R. Age, spreading rates and spreading symmetry of the world's ocean crust. *Geochemistry, Geophysics, Geosystems* **9** (2008).

56. D'Hondt, S.L., Jørgensen, B.B., Miller, D.J., et al. Proc. ODP, Init. Repts., 201: College Station, TX (Ocean Drilling Program) (2003).

57. Skilbeck, C.G., and Fink, D. Data report: Radiocarbon dating and sedimentation rates for Holocene– upper Pleistocene sediments, eastern equatorial Pacific and Peru continental margin. In Jørgensen, B.B., D'Hondt, S.L., and Miller, D.J. (Eds.), Proc. ODP, Sci. Results, 201, 1–15 (2006).

58. Guizhi, W. Arthur J. Spivack, Scott Rutherford, Uri Manor, and Steven D'Hondt. Quantification of co-occurring reaction rates in deep subseafloor sediments. *Geochimica et Cosmochimica Acta* **72**, 3479-3488 (2008).

59. D'Hondt, Steven, Fumio Inagaki, Carlos Alvarez Zarikian, Lewis J. Abrams, Nathalie Dubois, Tim Engelhardt, Helen Evans et al. Presence of oxygen and aerobic communities from sea floor to basement in deep-sea sediments. *Nature Geoscience* 8, 299-304 (2015).

60. Anderson, L.A. and Sarmiento, J.L. Redfield ratios of remineralization determined by nutrient data analysis. *Global biogeochemical cycles* **8**(1), 65-80 (1994).

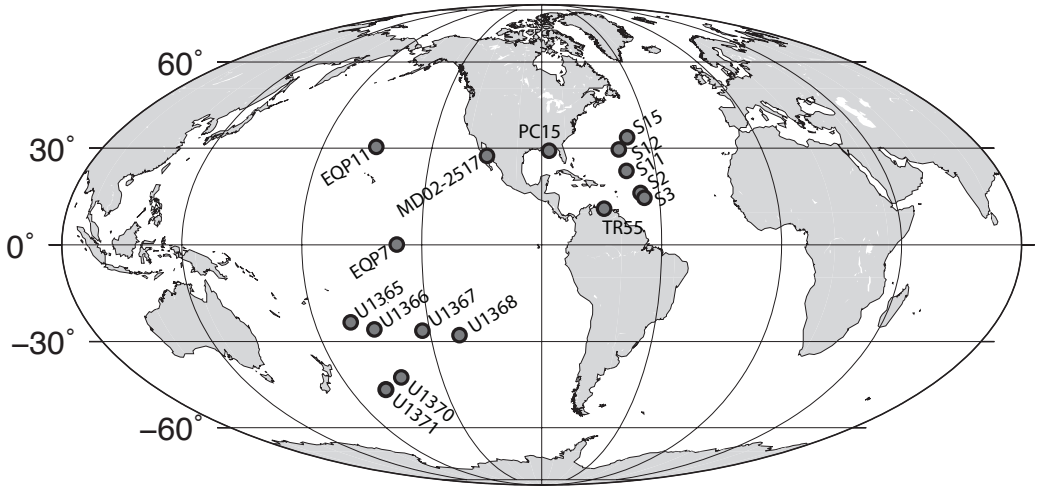

Figure 1.S1. Sample location for sediment samples used in the radiation experiments.

Collection locations for the marine sediment samples used in the radiation experiments.